Research Paper

THEMED ISSUE: Anatomy of Rifting: Tectonics and Magmatism in Continental Rifts, Oceanic Spreading Centers, and Transforms

GEOSPHERE

GEOSPHERE; v. 12, no. 1

doi:10.1130/GES01173.1

6 figures; 2 tables; 1 supplemental file

CORRESPONDENCE: nathens@stanford.edu

CITATION: Athens, N.D., Glen, J.M.G., Klemperer, S.L., Egger, A.E., and Fontiveros, V.C., 2016, Hidden intrabasin extension: Evidence for dike-fault interaction from magnetic, gravity, and seismic reflection data in Surprise Valley, northeastern California: Geosphere, v. 12, no. 1, doi:10.1130/GES01173.1.

Received 28 January 2014
Revision received 23 September 2015
Accepted 21 October 2015

Hidden intrabasin extension: Evidence for dike-fault interaction from magnetic, gravity, and seismic reflection data in Surprise Valley, northeastern California

Noah D. Athens[1,2,*], Jonathan M.G. Glen[1], Simon L. Klemperer[2], Anne E. Egger[3], and Valentina C. Fontiveros[2]

[1]U.S. Geological Survey, 345 Middlefield Road, Menlo Park, California 94025, USA
[2]Department of Geophysics, Stanford University, 397 Panama Mall, Mitchell Building, Stanford, California 94305, USA
[3]Department of Geological Sciences, Central Washington University, 400 E. University Way, Ellensburg, Washington 98926-7418, USA

ABSTRACT

The relative contributions of tectonic and magmatic processes to continental rifting are highly variable. Magnetic, gravity, and seismic reflection data from Surprise Valley, California, in the northwest Basin and Range, reveal an intrabasin, fault-controlled, ~10-m-thick dike at a depth of ~150 m, providing an excellent example of the interplay between faulting and dike intrusion. The dike, likely a composite structure representing multiple successive intrusions, is inferred from modeling a positive magnetic anomaly that extends ~35 km and parallels the basin-bounding Surprise Valley normal fault on the west side of the valley. A two-dimensional high-resolution seismic reflection profile acquired across the magnetic high images a normal fault dipping 56°E with ~275 m of throw buried ~60 m below the surface. Densely spaced gravity measurements reveal a <1 mGal gravity low consistent with the fault offset inferred from the seismic data. Collinearity of the magnetic high and gravity low for ~6 km implies normal fault control of the dike along that length. The unusually shallow angle of the dike suggests that motion along the fault (perhaps aided by reduced friction along the dike) and associated block rotation resulted in post-intrusion tilting of the dike. The source of the dike is likely related to a shallow brittle-ductile transition zone that was elevated following rapid slip on the Surprise Valley fault after 3 Ma. Prior to our work, the Surprise Valley fault was assumed to accommodate the vast majority of extension across the region. Our results indicate that subsurface features, although no longer active, are significant contributors to the processes, timing, and total amount of extension observed in continental rift environments.

INTRODUCTION

In continental rift zones such as the Basin and Range or East African Rift, tectonic extension in the seismogenic crust can be accommodated by normal faulting or magmatism. In active systems, satellite geodesy coupled with studies of seismicity can identify events in which rift-related extension is accommodated by diking (Wright et al., 2006; Pallister et al., 2010), seismic slip and aseismic deformation (Payne et al., 2008; Bell et al., 2012), or a combination (Calais et al., 2008; Biggs et al., 2009). When extension is accommodated by both magmatic and tectonics processes, the proportion of strain accommodated by each process as well as the spatial and temporal distribution of the two processes are highly variable.

In systems that are no longer active, geologic mapping can assess the spatial and temporal distribution of strain over a longer time period. For example, in Mono Basin (California) Bursik and Sieh (1989) mapped fault scarps and measured offset along them, and compared the timing of events with eruption of the Mono Craters; on the basis of these data sets, they hypothesized that extension was accommodated by normal faulting prior to 40 ka, and was supplanted by dike intrusion since then. Parsons and Thompson (1991) expanded this hypothesis into the axiom that normal faulting and magmatism work together to accommodate strain in proportion with the magma supply. Their model suggests that when there is sufficient magma supply, magmatic intrusion suppresses normal faulting. While this may be the case in a broad sense (e.g., Parsons et al., 1998), the relationship between magmatism and faulting appears to be more complicated at the scale of individual events or on shorter time scales. For example, Valentine and Krogh (2006) hypothesized that dikes intruding into preexisting faults may actually promote slip along those faults by reducing friction.

Determining the total amount and distribution of strain, as well as the relative timing and contributions of dike intrusion and normal fault slip, requires looking beyond surface exposures. The basins of the Basin and Range hide a significant portion of the deformational history of the region; several geophysical studies have shown that normal faults with significant offset are buried beneath alluvium (Langenheim et al., 2001; Grauch and Hudson, 2007; Blackwell et al., 2009). It can be particularly difficult to assess the role of magmatic intrusions such as dikes in the subsurface because their narrow, vertical form makes them essentially invisible to seismic reflection profiles. Potential field data can provide more insight in many areas where mafic dikes present a significant contrast in both density and magnetic properties with the sur-

*Present address: Department of Geological Sciences, Stanford University, 450 Serra Mall Building, Stanford, California 94305, USA

rounding rocks. In combination, seismic and potential field data are capable of producing detailed maps and models of the subsurface that facilitate a more complete strain analysis than can be determined from surface mapping.

The northwestern margin of the Basin and Range has been the subject of numerous geological studies in the past decade (Colgan et al., 2006; Meigs et al., 2009; Scarberry et al., 2010; Egger and Miller, 2011). In the Surprise Valley region in particular, 12%–15% extension over ~50 km has been documented through surface mapping of exposed faults (Egger and Miller, 2011). The estimated extension, however, did not take into account strain buried in the basin. The potential field and seismic reflection work presented here suggests that significant structures are hidden beneath the sediments of the basin, indicating not only more extension than has been previously estimated, but that a portion of that extension is occurring through dike intrusion. In addition, these intrabasin structures suggest a complex interaction between developing normal faults and dikes that may be influenced by a shallow brittle-ductile transition zone.

GEOLOGIC SETTING

Surprise Valley is an extensional basin located along the northwestern margin of the Basin and Range Province (Fig. 1). It is bound on the west by the Surprise Valley fault, which has accommodated ~8 km of dip-slip motion since the middle Miocene to expose a sequence of Eocene and younger volcanic and volcaniclastic rocks in the Warner Range (Egger and Miller, 2011). The northern part of the valley, referred to here as the upper basin, consists of a half-graben bound on the west by the Surprise Valley fault and by the Larkspur Hills to the east (Fig. 1). The Larkspur Hills consist of late Miocene–Pliocene (8–3 Ma) low-potassium, high-alumina olivine tholeiites interbedded with tuffs and tuffaceous sediments (Tbl), a sequence that crops out extensively in northeastern California and southern Oregon (Hart et al., 1984; Carmichael et al., 2006). Arc-derived Oligocene volcanic rocks (Tv), exposed to the south in the Hays Canyon Range and in the Warner Range to the west, underlie the basalts (Colgan et al., 2011).

The interbedded basalt flows and lake sediments that fill the basin generate strong contrasts ideally suited for geophysical methods. A potential field model was developed (Egger et al., 2010) along a seismic reflection profile (Fig. 1) acquired by Lerch et al. (2010); both the seismic profile and potential field model suggest the presence of numerous intrabasin faults with offsets to tens of meters. These buried faults are likely analogous to faults exposed east of the valley in the Larkspur Hills (Fig. 1), where numerous small-offset, east-dipping normal faults cut ca. 8–3 Ma basalts (Tbl), with a total extension of 5%–7% over 10 km (Strickley, 2014). These faults are no longer active, however, based on laterally continuous paleoshorelines that formed ca. 0.02 Ma (Egger, 2014). Strickley (2014) also mapped several linear volcanic vents that parallel fault trends, but did not observe any dikes. Ritzinger (2014) used paleomagnetic data to distinguish six distinct flow groups that were spatially controlled by normal faults, suggesting that normal faults developed concurrently (perhaps episodically) with volcanism.

Within Surprise Valley, a significant positive magnetic anomaly was imaged (Glen et al., 2013) that roughly parallels the orientation of the Surprise Valley fault, but is straighter and longer than any segment of it or any individual fault within the Larkspur Hills (Fig. 1B). Here we use potential field modeling that integrates data from gravity and magnetic profiles (Athens, 2011) with a high-resolution seismic reflection profile (Fontiveros, 2010) to examine the source of the magnetic high (Fig. 1).

GEOPHYSICAL METHODS

Magnetic Data

Ground-based magnetic measurements were collected (Athens, 2011; Glen et al., 2013) using a cesium-vapor magnetometer mounted on or towed behind all-terrain vehicles (Athens et al., 2011) as well as a backpack-mounted system. Processing steps included subtracting diurnal variations of the Earth's magnetic field, removing aberrant data points (either due to sensor error or cultural artifacts), and removing the International Geomagnetic Reference Field to derive the residual magnetic anomaly field (Fig. 1B). The data density is greatest in the upper basin and the central portion of the middle basin due to easy access to the playa and better terrain for the all-terrain vehicles. Detailed magnetic profiles in the upper basin are shown in Figure 2A.

Gravity Data

A detailed gravity survey complemented the magnetic survey in the upper basin; 313 gravity stations were collected along 17 east-west transects across the magnetic anomaly, with station spacing ranging from 50 to 250 m (Fig. 2B). Gravity stations were tied to a primary base station in Alturas, California (Jablonski, 1974), and were reduced using standard gravity methods that include Earth-tide, instrument drift, latitude, free-air, simple Bouguer, curvature, terrain, and isostatic corrections (e.g., Blakely, 1995).

Seismic Data

We acquired a high-resolution seismic reflection profile located over the narrowest portion of the magnetic high (Fig. 2) where the magnetic source is expected to be shallowest based on a simple rule-of-thumb depth-to-source calculation (Peter's method; e.g., Blakely, 1995). The reflection profile was shot using a Betsy Seisgun and collected with a 955 m cabled recording array with 8 linked, 24-channel Geometrics Geode Ultra-Light Exploration (www.geometrics.com) seismographs. Details of the seismometer array, shot spacing, and recording parameters were provided in Fontiveros (2010). The ideal conditions of fine-grained lake deposits saturated by water almost immediately below the surface enabled penetration depths to 400 m (Fontiveros, 2010).

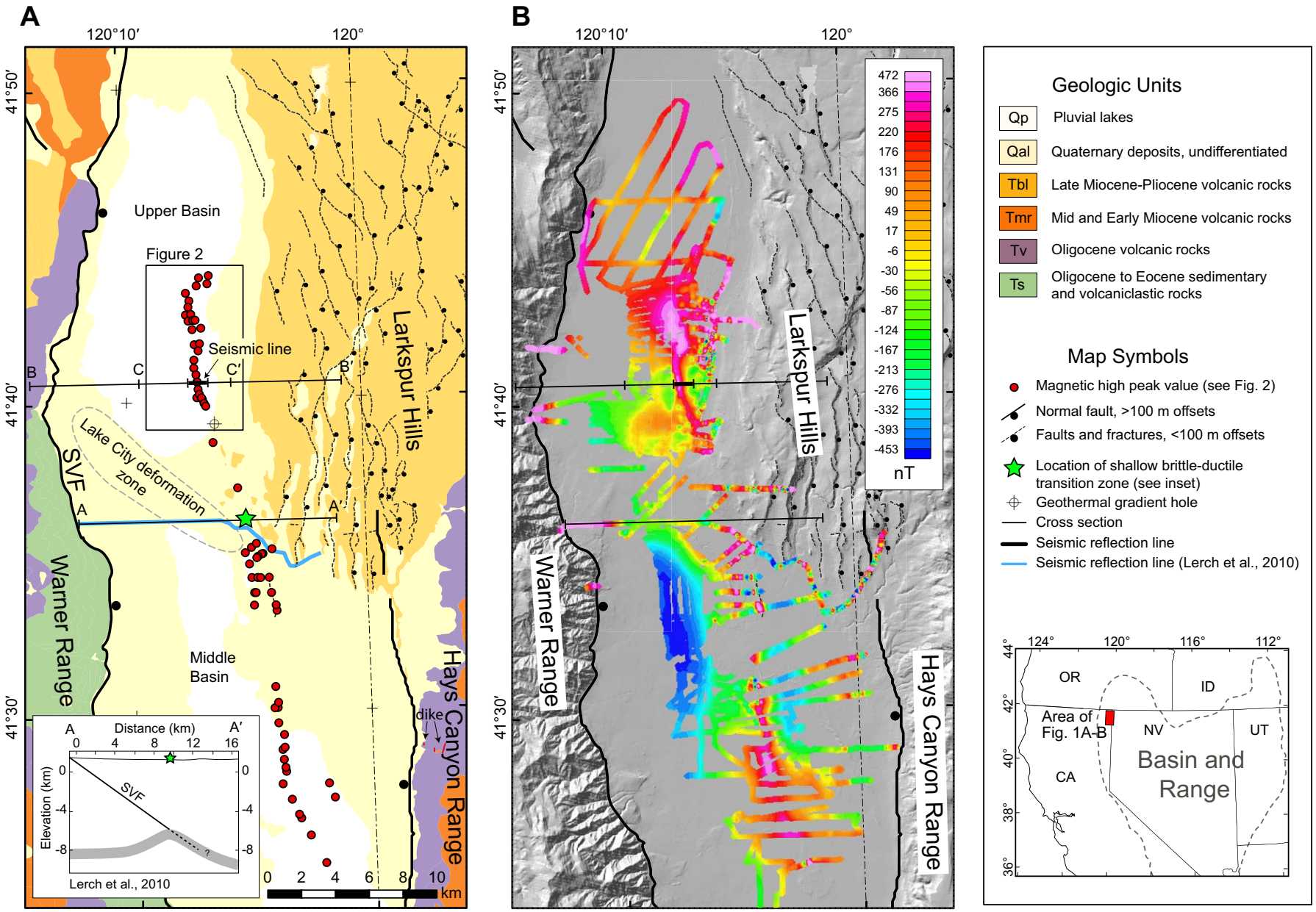

Figure 1. (A) Simplified geologic map of Surprise Valley in northeast California (modified from Egger and Miller, 2011; Egger et al., 2014). See legend for description of geologic units and map symbols. Cross-sections B–B′ and C–C′ are shown in Figure 3C. Inset (reproduced from Lerch et al., 2010) shows approximate depth of brittle-ductile transition zone along profile A–A′. SVF—Surprise Valley fault. (B) Shaded relief map and residual magnetic anomaly map (reproduced from Glen et al., 2013).

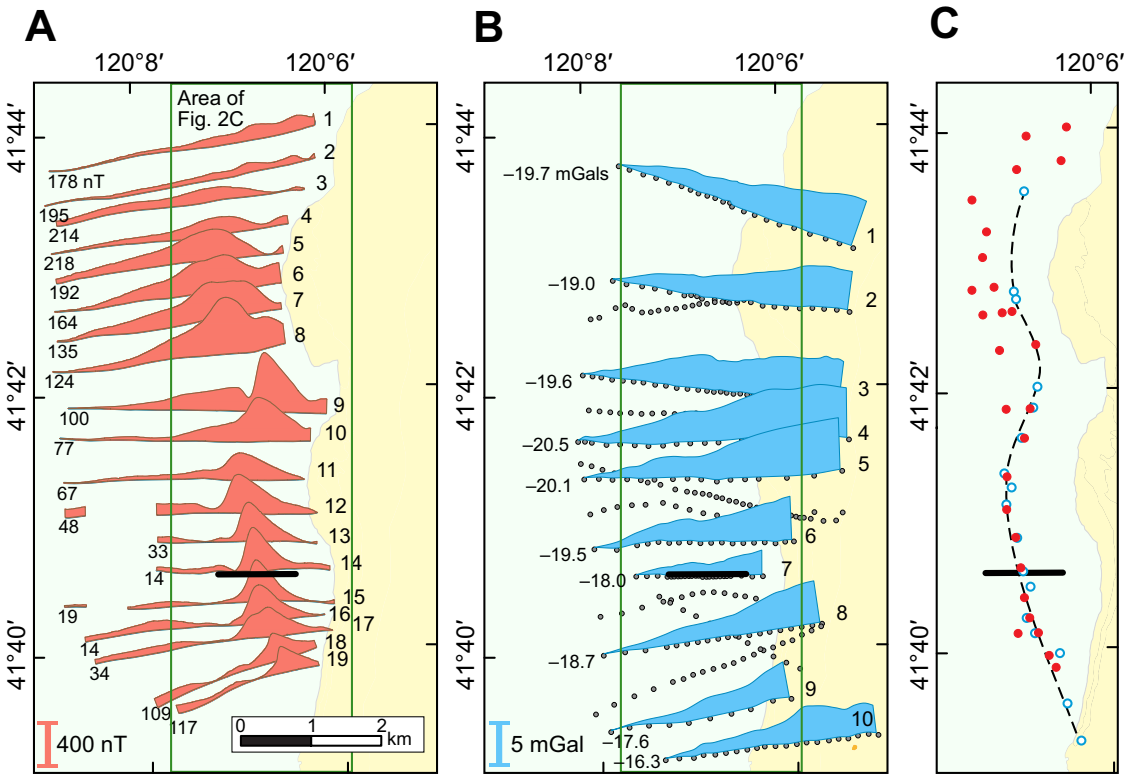

Figure 2. Magnetic and gravity profiles in the upper basin (location in Fig. 1). Profiles are plotted with the same dynamic range and centered for each profile (baseline values are indicated). Location of the seismic reflection profile (Fig. 3A) is shown by the thick black line. (A) Magnetic profiles. Magnetic data measurements acquired at ~1 m spacing. (B) Isostatic gravity profiles. Gravity data measurements (black circles) acquired at variable spacing, 50 m along seismic profile and 100–200 m elsewhere (7 profiles are not shown for clarity). (C) Manually selected magnetic high peak values (red circles) and gravity low (blue circles). Dashed line—inferred fault.

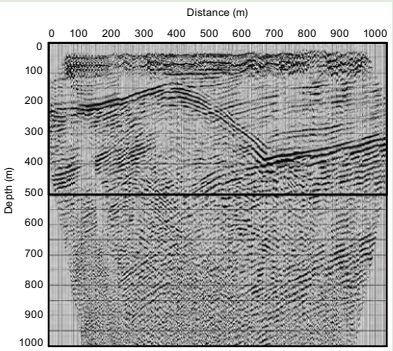

[1]Supplemental Figure 1. Unmigrated common midpoint stack. The high-amplitude reflection (B in Fig. 3A) is clearly homoclinal rather than synformal. Depth conversion is based on the velocity model of Figure 3A. Please visit http://dx.doi.org/10.1130/GES01173.S1 or the full-text article on www.gsapubs.org to view Supplemental Figure 1.

The acquired seismic data were processed using ProMAX seismic software. To address the variable frequency response of trace sections in the shot gathers (due to the two different types of geophones used), a 60–120 Hz bandpass filter was applied. Reverberations were suppressed using a predictive-deconvolution operator (60 ms operator length, 15 ms prediction distance). Amplitudes at depth were enhanced by applying a 175 ms automatic gain control. Airwave frequencies in the data set were similar to significant reflections (~60–80 Hz); therefore, instead of filtering out the airwave, we applied a bottom mute (all samples recorded after the onset of the ground-roll were set to zero on each trace) that removed both the ground roll and the airwave. In addition, refractions at the top of the record were muted so only reflection energy was processed and stacked. A detailed velocity analysis was performed to characterize the complex lateral velocity variations, and a normal moveout correction was applied. The data were migrated using Kirchhoff pre-stack depth migration (Fontiveros, 2010). Our interpretation utilized both the migrated (Fig. 3A) and the unmigrated (see Supplemental Fig. 1[1]) sections.

RESULTS

The magnetic anomaly map reveals an isolated, ~35-km-long, nearly continuous magnetic high (Fig. 1B). The majority of the high is <500 m wide, although the northern and southern extents broaden to a width of 1–2 km. Profiles across the high show that its amplitude, wavelength, and shape are highly variable despite its continuity (Fig. 2A). In the northern profiles (lines 5–8) where the high is broadest, the shape is asymmetric with a gentle gradient west of the peak and a steeper gradient to the east. In the southern profiles (lines 11–19) the sense of asymmetry is opposite. In lines 9 and 10, the peaks of the high are 50 and 100 m east of the trend from other profiles, and several profiles have multiple peaks (lines 6, 7, 8, 9, and 17). Given its isolation from other anomalies (Fig. 1B), the variability within the anomaly is likely a primary feature of the causative body rather than due to interactions with other magnetic sources.

Gravity profiles reveal an ~0.5 mGal low within a long-wavelength gradient (Fig. 2B). The trace of the gravity low is colocated with the peak of the

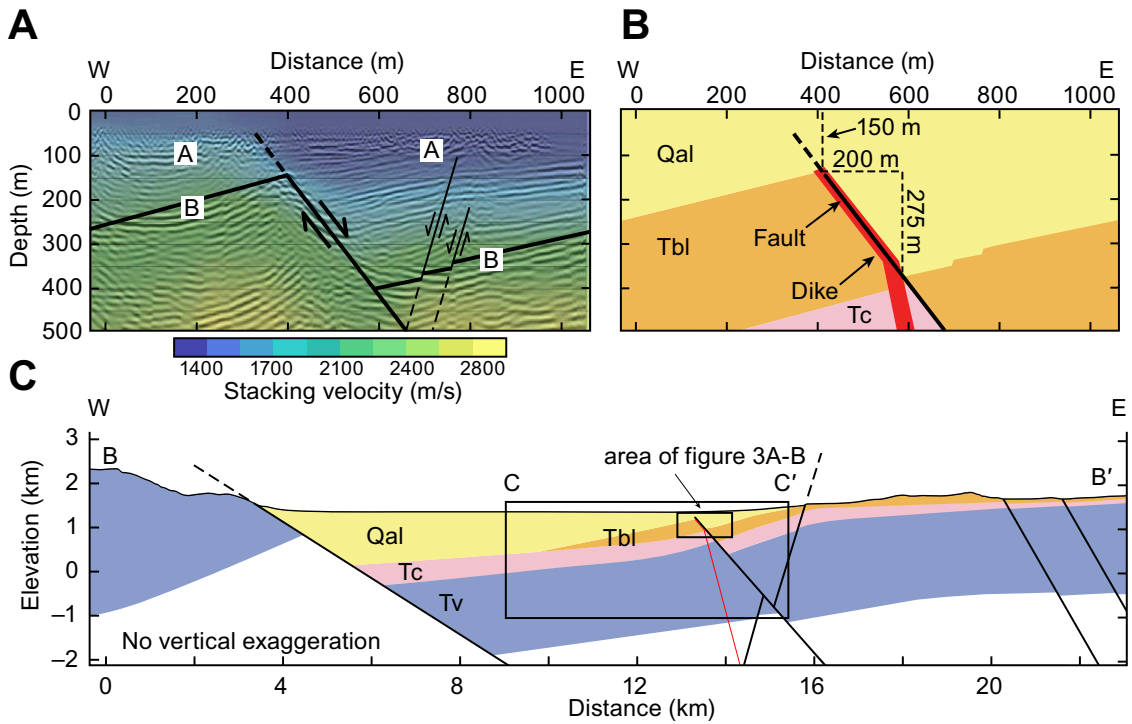

Figure 3. (A) Seismic cross section (location in Fig. 1A). Seismic image is a pre-stack depth migration with velocity model overlay (1400–2800 m/s, as indicated by the color key). Reflection symbols: A—lacustrine and playa deposits; B—Pliocene capping basalt. Fault dip is 56°. Interpretation is shown by black lines. (B) Interpretation of seismic cross section. (C) West-east cross section along B–B′ (Fig. 1). Geologic units as in Figure 1. C–C′ is an area of cross section of Figure 5.

magnetic high for ~6 km, but is east of the magnetic high where it broadens to the north (Fig. 2C).

In the seismic reflection profile, the highest amplitude reflection (B in Fig. 3A) appears between 200 and 400 m depth, dips westward, and is laterally discontinuous, offset ~340 m (dip-slip down to the east) in the middle of the profile. Both west and east of the offset, reflection B has a synformal shape that likely represents "smiles," artifacts that result from migrating seismic data that are imperfect (e.g., Warner, 1987). In our data the limited line length did not capture the full amplitude response of reflection B at either end of the profile, and attenuation prevented imaging the complete diffractions where B is offset (Supplemental Fig. 1). We therefore interpret reflection B as homoclinal (Fig. 3A) as the simplest interpretation consistent with the data. Above reflection B to ~100 m depth is a zone of low-amplitude west-dipping reflections (A in Fig. 3). No reliable reflections are imaged below reflection B, likely due to seismic ringing on a thick basalt layer.

Modeling Along Seismic Profile

In order to differentiate between possible sources of the magnetic high, we developed two-dimensional potential field forward models along the seismic profile using a commercial two-dimensional forward modeling package (GM-SYS; www.geosoft.com). Because modeling solutions of potential field anomalies are nonunique, the highest amplitude reflection in the seismic data (B in Fig. 3) served as a key constraint. Physical property data (density, magnetic susceptibility, and magnetization measurements) collected from surface samples also provided important constraints for the modeling process. The values employed in the models (Tables 1 and 2) are primarily based on published physical property measurements (Ponce et al., 2009) and paleomagnetic measurements (Ritzinger, 2014) of units exposed at the surface in closest proximity to the model. In some cases, however, modeled layers cannot be sampled, or the use of known physical properties was not sufficient to match the observations, so in these cases, physical property values are estimated (these values are described where relevant).

Most exposed basalt flows in the area are reversely magnetized, although normal and transitional flows are also present (Ritzinger, 2014). A 292-m-deep geothermal gradient hole located 5 km south of the seismic profile along the magnetic high (Fig. 1) recovered reversely magnetized basalt core from 88 to 89 m depth and 143 to 145 m depth (J. Glen, personal data), while the rest of the

TABLE 1. SUMMARY OF PHYSICAL PROPERTY DATA USED IN TWO-DIMENSIONAL MODELS

	Mean physical property measurements†			Density and magnetic properties used in final two-dimensional model		
Rock unit*	Number of samples	Density range (g/cm³)	Mean density (g/cm³)	Density values (g/cm³)		
Qal	5	1.53–2.08	1.74	1.9, 2.14, 2.3		
Tbl	23	2.46–2.93	2.76	2.4		
Tc	ND	ND	ND	2.1		
Tv	46	2.02–2.90	2.49	2.55, 2.65		
Dike	ND	ND	ND	2.67		
Rock unit	Number of samples	*k* range (SI x 10³)	Mean *k* (SI x 10³)	*k* range (SI x 10³)	M values (A/m)	Polarity§
Qal	5	0.63–1.68	1.0	0, 0, 1	0, 0, 0.004	N
Tbl	23	0.32–6.48	2.3	3	1.44	R
Tc	ND	ND	ND	4	0.3	N
Tv	46	0.07–26	8.6	25	1	N
Dike	ND	ND	ND	25	10	N

Note: Description of how physical property measurements were applied to the models is given in the text. ND—no data; *k*—magnetic susceptibility; M—magnetic remanence.

*Qal—Quaternary alluvium, undifferentiated; Tbl—late Miocene–Pliocene volcanic rocks; Tc—middle and early Miocene tuffaceous sediment; Tv—Oligocene volcanic rocks.

†Ponce et al. (2009).

§N—normal; R—reversed.

core comprised sediments. To account for sediments interbedded in the basalts and for rubbly vesiculated layers between individual flows, physical property values for the basalt layer (Tbl) were calculated assuming that 50% of the layer had the properties of alluvium (Qal), which is less dense and less magnetic (Table 1).

Given the region's history of extension and associated volcanism, there are limited geologically consistent possibilities for the structures and associated features likely to appear in the subsurface. For that reason, we considered three possible end-member models for the source of the magnetic high: (1) the normal fault model, which relies on faulted magnetic stratigraphy, (2) the ponded basalt model, where basalt flows fill faulted topography, and (3) the dike model, which relies on a mafic intrusion. End-member models are useful to determine the primary influences on the source of the anomaly, even if particular models are known to be incorrect, incomplete, or problematic. As described in the following section, the first step in the modeling process was to determine the characteristic magnetic and gravity fields produced by these end-member structures (Fig. 4). While these models are simplistic, they show that the end-member sources produce very distinct anomalies.

Results of End-Member Models

Our normal fault model (Fig. 4A) depicts a west-dipping magnetic layer that is cut and offset by an east-dipping fault based on offset reflections in the seismic profile that we interpret to be the top of the late Miocene–Pliocene basalts (Tbl). The transition from Quaternary lacustrine deposits to basalt provides the acoustic contrast necessary to produce the high-magnitude reflection. The dip of the Tbl layer produces a gentle gravity gradient that reflects the shape of the basin (Fig. 4A). Within the gravity gradient, the offset of the Tbl layer produces a gravity low where less dense alluvium (Qal) fills in above the hanging wall. The depth and orientation of Oligocene volcanics (Tv) were estimated by projecting mapped units (from Egger and Miller, 2011) into the subsurface, although this layer has relatively little influence in the model. This model correctly produces the observed gravity profile; therefore, an interpretation of a fault from the seismic data is supported by the gravity data. The fit of the magnetic data, however, is poor. In the first calculation (red line in Fig. 4A), magnetic parameters used for the Tbl layer (Table 2) are based on our best estimate from magnetic susceptibility and remanence measurements (Ritzinger, 2014), taking into account less magnetic sediment that is interbedded in the basalt. In the second calculation (blue dashed line in Fig. 4A), maximum magnetic parameters are used (Table 2) based on the upper end of measured magnetic values (Ritzinger, 2014). In both cases, however, the calculated magnetic high is not of sufficient amplitude.

In our ponded basalt model (Fig. 4B), we added a highly magnetic layer that conceptually represents a basalt flow (Tpb) that pooled on the hanging wall of the faulted topography (Fig. 4B); otherwise, this model is equivalent to the normal fault model using the best estimate for the Tbl layer's magnetic parameters. In the first calculation (red line in Fig. 4B), the resulting magnetic profile is virtually unchanged from the normal fault model (Fig. 4A), due to the Tpb layer's planar horizontal orientation and magnetic parameters that are similar to those of the Tbl layer (Table 2). In the second calculation (blue dashed line in Fig. 4B), changing the Tpb layer from normal to reversed polarity has the effect of increasing the amplitude of the magnetic high, which is closer to fitting the observed high (Fig. 4B). This model, however, is inconsistent with the seismic profile. If a pooled basalt flow were present in the thickness indicated in the model, we would expect it to appear in the seismic reflection profile.

Our dike model (Fig. 4C) shows a 10-m-thick dike in two orientations, vertical and east dipping, intruding horizontal stratigraphy. Although this does not conform to the dipping, faulted reflections in the seismic data, our intent was to assess the gravity and magnetic contributions of the dike alone rather than the faulted stratigraphy that is already depicted in the first two models. The dike is assumed to be highly magnetic and dense, similar

TABLE 2. PHYSICAL PROPERTIES FOR THE GEOLOGIC UNITS IN THE TWO-DIMENSIONAL MODELS

Model unit	Unit description	End-member models: Normal fault (Fig. 4A) Calc.1	Normal fault (Fig. 4A) Calc. 2	Ponded basalt (Fig. 4B) Calc. 1	Ponded basalt (Fig. 4B) Calc. 2	Dike (Fig. 4C) Calc. 1	Dike (Fig. 4C) Calc. 2	Final model (Fig. 5)
Qal	Quaternary deposits 0-300 m	ρ = 2, *k* = 0, M = 0						ρ = 1.9, *k* = 0, M = 0
Qal	Quaternary deposits 300-700 m	ρ = 2, *k* = 0, M = 0						ρ = 2.14, *k* = 0, M = 0
Qal	Quaternary deposits 700-1000 m	ρ = 2, *k* = 0, M = 0						ρ = 2.3, *k* = 1, M = 0.004
Tpb	Pliocene basalt flow			ρ = 2.7, *k* = 6, M = 3	ρ = 2.7, *k* = 6, M = 3			
Dike	Mafic dike					*vertical*	*dipping* ρ = 2.7, *k* = 25, M = 10	ρ = 2.67, *k* = 25, M = 10
Tbl	Late Miocene-Pliocene volcanic rocks	ρ = 2.4, *k* = 3, M = 1.4	ρ = 2.4, *k* = 6, M = 3	ρ = 2.4, *k* = 3, M = 1.4		ρ = 2.4, *k* = 0, M = 0		ρ = 2.4, *k* = 3, M = 1.44
Tc	Mid and early Miocene tuffaceous sediment							ρ = 2.1, *k* = 4, M = 0.3
Tv	Oligocene volcanics 1000-2000 m	ρ = 2.7, *k* = 25, M = 1						ρ = 2.55, *k* = 25, M = 1
Tv	Oligocene volcanics > 2000 m	ρ = 2.7, *k* = 25, M = 1						ρ = 2.65, *k* = 25, M = 1

Note: Calc—calculated field; ρ—density (g/cm^3); *k*—magnetic susceptibility (SI x 10^3); M—magnetic remanence (A/m). Magnetic remanence direction: normal polarity is assumed to be 65° inclination, 0° declination; reversed polarity (indicated in red) is assumed to be –65° inclination, 180° declination.

in rock properties to a subsurface flow modeled by Egger et al. (2010). For convenience we have modeled the dike as a single, rectangular block, while recognizing that dikes generally thin toward the tip (e.g., Gudmundsson, 2003) and that at 10 m thickness, the dike may be a composite structure representing multiple successive intrusions. The depth to the top of the dike was chosen in order to minimally contribute to the gravity field (i.e., there is no observed gravity high). In the first calculation (red line in Fig. 4C), the magnetic high produced by the vertical dike does not match the sense of asymmetry of the observed magnetic high, which has a steeper gradient on the western side of the high. In the second calculation (blue dashed line in Fig. 4C), the sense of asymmetry matches the observed high more closely.

Final Model

As expected, none of the end-member models reproduce the observed high-amplitude magnetic high aligned with a gravity low. However, by combining the normal fault model (Fig. 4A) and the dipping dike model (Fig. 4C) into a single model, both the asymmetric high-amplitude magnetic high and gravity low can be reproduced (Fig. 5). The gravity fit was further improved by the addition of two alluvium layers (Qal) that increase the density of alluvium with depth, consistent with typical basin sediment depth profiles (Brocher, 2008). A low-density tuffaceous sediment layer (Tc) was also added to the model, consistent with tuffs modeled (by Egger et al., 2010) along the nearby seismic line acquired by Lerch et al. (2010) (Fig. 1A).

DISCUSSION

Nature and Development of the Magnetic Anomaly

Colocation of a magnetic high with a gravity low is unusual because of the common association of high magnetizations with high-density mafic bodies. Therefore, no end-member potential field model (Fig. 4) accurately reproduces the anomalies in Surprise Valley. Even if a single causative body were able to produce the magnetic high and gravity low along the seismic profile, the broadening of the magnetic high to the north and its divergence from the gravity low (Figs. 1 and 2) would preclude such a model. Instead, only a model that combines a normal fault with a dike fits the observed gravity, magnetic, seismic, and geologic data (Fig. 5).

The ~10 m thickness and ~150 m depth of the dike, as well as its relationship to the fault, are only partially constrained by the modeling. In order to fit the observed gravity low, the sole constraint on the dike is that it must be sufficiently thin and deep that it does not produce a gravity anomaly (Fig. 4C). However, because the proportion of thickness to depth may vary, and because the dike cannot be sampled for physical properties, the dike's thickness and depth may vary by tens of meters without affecting the gravity fit. Nevertheless, the ~10 m thickness is consistent with displacement length scaling relations that predict a maximum opening of 13 m for a 35-km-long dike (Schultz et al., 2008, fig. 5 therein). Furthermore, the location of the top of the dike at the contact between the basalt (Tbl) and sediment (Qal) is reasonable given field observations and modeling of dike arrest in layered crust (Gudmundsson, 2002).

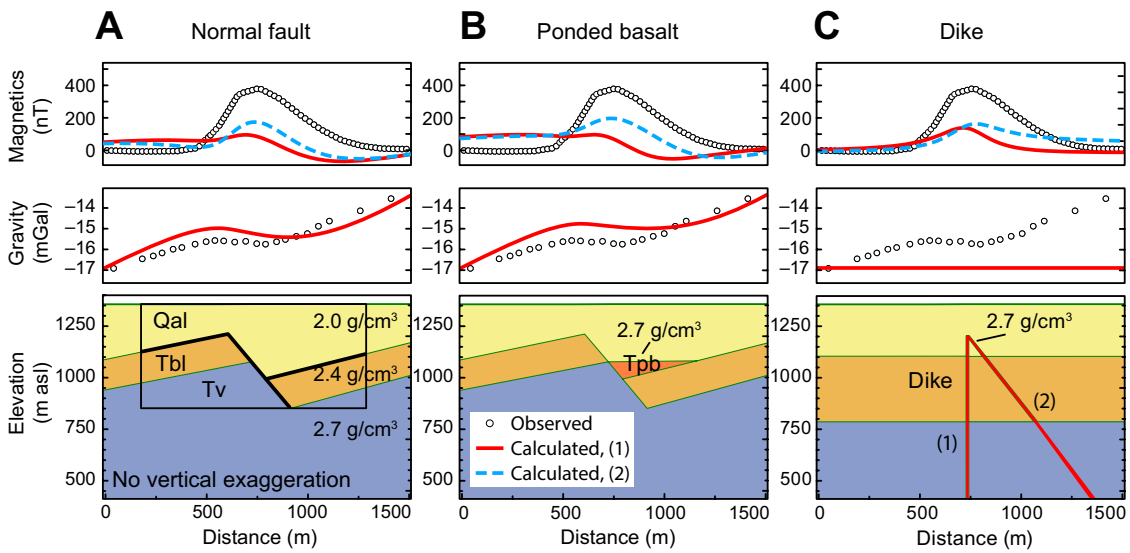

Figure 4. End-member potential field models along seismic reflection profile. Extent of seismic cross section (Fig. 3A) is shown by black box (asl—above sea level). Physical property values are indicated in Table 2. Geologic units as in Figure 1, except for Tpb (described in text). (A) Normal fault model. (B) Ponded basalt model. (C) Dike model. The second calculated gravity field is equivalent to the first because all densities are held constant, and therefore the blue dashed line is not visible in the gravity models.

Given the relatively shallow dip of the dike and its interaction with the fault, a key question is whether this scenario is likely, based on the processes of diking and faulting. Valentine and Krogh (2006) observed fault-captured dikes in Paiute Ridge, Nevada, finding that the dikes, 400–5000 m long and 1.2–9 m thick, only occupied normal faults that were steeper than 60°. Their field observations are supported by analytic and numerical modeling (Gaffney et al., 2007), which find that in addition to steep fault angles, fault capture of propagating dikes becomes more favorable at shallow depths and with high fracture toughness in the hanging wall. Assuming that the basalts (Tbl) have a fracture toughness of 1 MPa $m^{1/2}$, which is likely an underestimate (Gaffney et al., 2007, Table 1 therein), and the fault dip angle is 60°, fault capture of a rising dike is permitted at depths <300–800 m, depending on preexisting cracks in the hanging wall. Although the fault in our model dips 56° to the east (shallower than expected for dike capture), stratigraphy dips 15° to the west, indicating that the fault probably formed at an angle as steep as 71° and, as is typical of normal faults in the Basin and Range, rotated to lower dips as motion occurred (Chamberlin, 1983). The dike could have been captured at any point during rotation of the fault plane.

We also note that the dike is located ~8–10 km east of the main trace of the Surprise Valley fault, and is roughly parallel to the fault along its length. This places the dike and magnetic anomaly directly above the location of a predicted shallowing of the brittle-ductile transition (inset, Fig. 1A) (Lerch et al., 2010). A rise of this transition zone by as much as 3 km may have occurred during a period of rapid slip on the Surprise Valley fault after 3 Ma (Colgan et al., 2008), a suggestion supported by flexure observed in the Warner Range (Egger and Miller, 2011) and high heat flow in the basin (Blackwell et al., 1991; Benoit et al., 2005). The location of the dike is consistent with where decompression melting would most likely occur.

On the basis of these geological constraints, we have developed a conceptual model for the sequence of events leading to the observed phenomena (Fig. 6). In our schematic diagram, a steeply dipping normal fault forms in the crust in response to basin extension ca. 3 Ma; motion along the fault results in minor offset of late Miocene–Pliocene basalts (Tbl), indicating that faulting initiated after

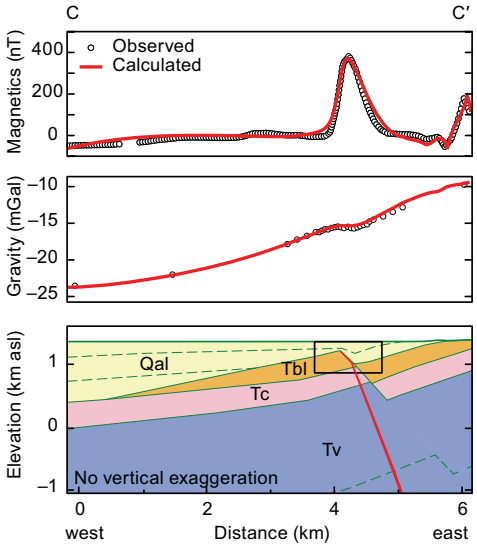

Figure 5. Final potential field model along line C–C′ in Figure 1. Extent of seismic reflection cross section (Fig. 3A) is shown by black box (asl—above sea level). Dashed line indicates density boundary (Table 2). Geologic units as in Figure 1; Tc—middle and early Miocene tuffaceous sediment inferred from modeling (see text).

3.8 Ma (Fig. 6A). Around the same time, rotation of the Surprise Valley fault and rapid uplift of the Warner Range raised the brittle-ductile transition zone (Lerch et al., 2010), generating the magma supply for dike intrusion. A dike rose subvertically through the crust and encountered the mechanically strong Miocene–Pliocene basalts in the shallow subsurface; as the dike moved through this strong layer, it was captured and diverted by the normal fault (Fig. 6B). Upon rising to the contact between the basalt and soft sediment just below the paleosurface, the dike was arrested (Fig. 6B). The age of the dike is not well known. An older age, during the post–3 Ma episode of rapid offset of the Surprise Valley fault, implies that the dike would have encountered the fault prior to significant tilt, and would have been likely to be captured by the fault. A younger age would have allowed greater accumulation of soft sediment above the fault tip, increasing the probability of dike arrest in the subsurface rather than eruption onto the paleolakebed (although examples are known where dikes were arrested within 5 m of the surface; Gudmundsson, 2003). Continued motion along the fault (Fig. 6C) and ongoing sedimentation resulted in tilting of the dike within the fault block and fanning of sedimentary deposits (Fig. 6D).

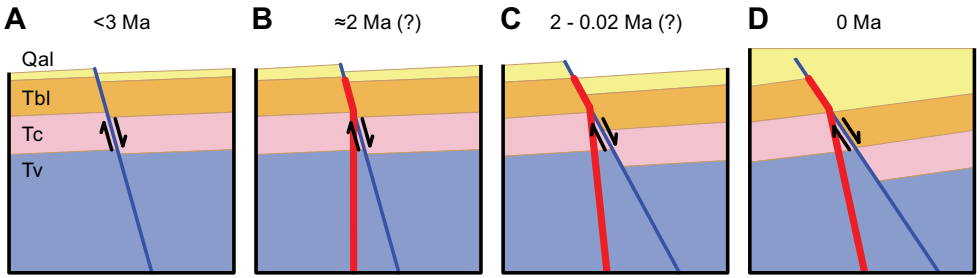

Figure 6. Schematic diagram of emplacement of synextensional, fault-captured dike. Geologic units as in Figure 1; Tc—middle and early Miocene tuffaceous sediment. (A) Predating dike emplacement, gently dipping strata are offset by high-angle, east-dipping normal fault. (B) Fault plane is exploited by a vertically rising dike that is arrested in soft sediment below the paleosurface. (C) Motion along the dike and rotation of the fault block occur. (D) Fault dips at its present 56°, while deposition of alluvium occurs.

Extension in the Basin

Utilizing the results from our modeling, the extent of the seismically imaged and modeled fault can be mapped using the small gravity low as a proxy for its location (Fig. 2C). By connecting the location of the gravity low along several transects, we interpret the buried fault to have an orientation similar to east-dipping faults located to the east in the Larkspur Hills (Fig. 1), which range in strike from 350° to 010° (Strickley, 2014). In Egger and Miller (2011), ~7.3 km of east-west extension across 50 km (or 15% extension) was calculated based on geologic mapping and offset calculations along exposed faults, including the Surprise Valley fault and several regional faults. Strickley (2014) calculated extension along several profiles across the Larkspur Hills, finding ~460 m of east-west extension across 10 km (or 5% extension) at the latitude of our model. In comparison, the fault in our model accommodates 200 m of horizontal slip (Fig. 3B). While this alone is not a significant amount of extension, it is possible that there are additional, as yet unidentified, intrabasin faults whose combined slip may accommodate a sizable amount of extension.

Geophysical work in other valleys throughout the Basin and Range suggest that multiple intrabasin faults are likely (e.g., Okaya and Thompson, 1985). Our densely spaced gravity data, which targeted the magnetic high, did not extend far enough into the basin to reveal additional intrabasin faults, and existing regional gravity coverage (Ponce et al., 2009) on a 1.6 km grid is not sufficient to reveal faults that cause <1 mGal anomalies. Furthermore, deeper, basinward faults would produce a significantly smaller gravity signal that may preclude their detection by gravity alone. One way to estimate the number and size of faults that may exist in the basin is to assume that the fault population follows a fractal size distribution (Marrett and Allmendinger, 1992). Based on the average 2 km lateral spacing of faults in the Larkspur Hills (Strickley, 2014) and the intrabasin fault identified in the reflection data, we estimate that there could be 5–10 more faults in the basin resulting in 1–2 km of additional extension hidden beneath the playa, and regional extension of 16%–19%. As a result, extension calculations in the Surprise Valley region likely underestimate the total extension that has occurred. These results have broader implications for similar extensional basins that remain concealed under basin sediments and have not been characterized geophysically.

Implications Along Strike of the Anomaly

The results from our modeling also provide a basis for interpreting complex features in the magnetic data throughout the basin. Between the middle and upper basins, the magnetic high crosses a region previously referred to as the Lake City fault zone or Lake City fault (Fig. 1A) (Hedel, 1980; U.S. Geological Survey and California Geological Survey, 2006) that was widely cited as an important throughgoing structural element controlling geothermal circulation in the valley. However, it was concluded (Egger et al., 2014) that the region lacks a throughgoing fault on the basis that there is no consistent gravity, magnetic, or resistivity signature coinciding with the fault, and therefore should not be mapped as such. Our results support this interpretation; we see clear continuity of the magnetic high across the zone with no evidence of offset within this region or elsewhere along the length of the anomaly. There is, however, evidence of structural complexity in the shallow subsurface where the magnetic high is more diffuse, consistent with the presence of a deformation zone, such

as may develop where faults interact, as suggested in Egger et al. (2014).

The broadening of the magnetic anomaly at its northern and southern extent (Fig. 1B) may be the result of the dike rising into more complex structure in the shallow subsurface (e.g., Keating et al., 2008). In the upper basin, the magnetic high not only broadens in the northern profiles, but also subtly changes in the sense of asymmetry and, in some profiles, has multiple peaks (Fig. 2A), suggesting that the dike is no longer controlled by a single east-dipping fault. Preliminary modeling suggests that the dike may be rising into a small horst or broader fault zone (Athens, 2011), although the lack of seismic reflection or well-log data means that the modeling is poorly constrained.

CONCLUSIONS

The acquisition of multiple, complementary geophysical data sets provided insight into subsurface features in Surprise Valley as it allowed us to identify features that are common across data sets or unique to one data set. Our combined analysis of geophysical data and modeling identifies a fault-controlled ~10-m-thick dike at a depth of ~150 m. The location of the dike, ~8–10 km east of the main trace of the Surprise Valley fault, corresponds to an area of a predicted elevated brittle-ductile transition zone (Lerch et al., 2010), which is precisely where decompression melting and diking would occur. The concealed fault, imaged by reflection data, is located 3 km west of the eastern edge of the basin and accounts for an additional ~200 m of extension. A further 1–2 km extension along unsampled intrabasin faults is considered possible based on the expected fault population.

Our results indicate that structures and magmatic features in the subsurface are important contributors to a complete assessment of the processes, timing, and total amount of extension observed in continental environments. Only through combined geological and geophysical analyses can we get a complete picture of the extensional history of regions such as the northwestern Basin and Range.

ACKNOWLEDGMENTS

We are indebted to all the volunteers who helped collect data, in particular Claire Bouligand, Bruce Chuchel, Kevin Denton, Nate Levine, Erin Looby, Nellie Olsen, and Alex Yu. We also thank Rick Blakely, Agust Gudmundsson, Francesco Mazzarini, and one anonymous reviewer for providing comments that greatly improved the manuscript. Magnetic and gravity acquisition was funded by the U.S. Geological Survey and Stanford University. Seismic data acquisition was funded by Stanford University, using recording equipment from the IRIS-PASSCAL (Incorporated Research Institutions for Seismology–Portable Array Seismic Studies of the Continental Lithosphere) equipment pool. Landmark Geophysical generously donated the ProMAX software license used for reflection processing.

REFERENCES CITED

Athens, N.D., 2011, Potential field modeling of intra-basin faulting in Surprise Valley, California [M.S. thesis]: Stanford, California, Stanford University, 110 p.

Athens, N.D., Glen, J.M.G., Morin, R.L., and Klemperer, S.L., 2011, ATV magnetometer systems for efficient ground magnetic surveying: The Leading Edge, v. 30, p. 394–398, doi:10.1190/1.3575284.

Bell, J.W., Amelung, F., and Henry, C.D., 2012, InSAR analysis of the 2008 Reno-Mogul earthquake swarm: Evidence for westward migration of Walker Lane style dextral faulting: Geophysical Research Letters, v. 39, L18306, doi:10.1029/2012GL052795.

Benoit, D., Moore, J., Goranson, C., and Blackwell, D.D., 2005, Core hole drilling and testing at the Lake City, California, geothermal field: Geothermal Resources Council Transactions, v. 29, p. 203–208.

Biggs, J., Amelung, F., Gourmelen, N., Dixon, T.H., and Kim, S.W., 2009, InSAR observations of 2007 Tanzania rifting episode reveal mixed fault and dyke extension in an immature continental rift: Geophysical Journal International, v. 179, p. 549–558, doi:10.1111/j.1365-246X.2009.04262.x.

Blackwell, D.D., Steele, J.L., and Carter, L.S., 1991, Heat-flow patterns of the North American continent: A discussion of the geothermal map of North America, *in* Slemmons, D.B., et al., eds., Neotectonics of North America: Boulder, Colorado, Geological Society of America, Decade Map Volume 1, p. 423–436.

Blackwell, D.D., Smith, R.P., Waibel, A., Richards, M.C., and Step, P., 2009, Why Basin and Range systems are hard to find II: Structural model of the producing geothermal system in Dixie Valley, Nevada: Geothermal Resources Council Transactions, v. 33, p. 441–446.

Blakely, R.J., 1995, Potential theory in gravity and magnetic applications: Cambridge, UK, Cambridge University Press, 464 p.

Brocher, T.M., 2008, Compressional and shear-wave velocity versus depth relations for common rock types in northern California: Seismological Society of America Bulletin, v. 98, p. 950–968, doi:10.1785/0120060403.

Bursik, M., and Sieh, K., 1989, Range front faulting and volcanism in the Mono Basin, eastern California: Journal of Geophysical Research, v. 94, p. 15,587–15,609, doi:10.1029/JB094iB11p15587.

Calais, E., et al., 2008, Strain accommodation by slow slip and dyking in a youthful continental rift, East Africa: Nature, v. 456, p. 783–787, doi:10.1038/nature07478.

Carmichael, I.S.E., Lange, R.A., Hall, C.M., and Renne, P.R., 2006, Faulted and tilted Pliocene olivine-tholeiite lavas near Alturas, NE California, and their bearing on the uplift of the Warner Range: Geological Society of America Bulletin, v. 118, p. 1196–1211, doi:10.1130/B25918.1.

Chamberlin, R.M., 1983, Cenozoic domino-style crustal extension in the Lemitar Mountains, New Mexico: A summary, *in* Chapin, C.E., and Callender, J.F., eds., Socorro region II: New Mexico Geological Society 34th Field Conference Guidebook, p. 111–118.

Colgan, J.P., Dumitru, T.A., Reiners, P.W., Wooden, J.L., and Miller, E.L., 2006, Cenozoic tectonic evolution of the Basin and Range Province in northwestern Nevada: American Journal of Science, v. 306, p. 616–654, doi:10.2475/08.2006.02.

Colgan, J.P., Shuster, D.L., and Reiners, P.W., 2008, Two-phase Neogene extension in the northwestern Basin and Range recorded in a single thermochronology sample: Geology, v. 36, p. 631–634, doi:10.1130/G24897A.1.

Colgan, J.P., Egger, A.E., John, D.A., Cousens, B., Fleck, R.J., and Henry, C.D., 2011, Oligocene and Miocene arc volcanism in northeastern California: Evidence for post-Eocene segmentation of the subducting Farallon plate: Geosphere, v. 7, p. 733–755, doi:10.1130/GES00650.1.

Egger, A.E., 2014, Paleoearthquake magnitudes derived from lidar-based mapping of fault scarps in the northwestern Basin and Range: Geological Society of America Abstracts with Programs, v. 46, no. 6, paper 323-5, p. 777.

Egger, A.E., and Miller, E.L., 2011, Evolution of the northwestern margin of the Basin and Range: The geology and extensional history of the Warner Range and environs, northeastern California: Geosphere, v. 7, p. 756–773, doi:10.1130/GES00620.1.

Egger, A.E., Glen, J.M.G., and Ponce, D.A., 2010, The northwestern margin of the Basin and Range province part 2: Structural setting of a developing basin from seismic and potential field data: Tectonophysics, v. 488, p. 150–161, doi:10.1016/j.tecto.2009.05.029.

Egger, A.E., Glen, J.M.G., and McPhee, D.K., 2014, Structural controls on geothermal circulation in Surprise Valley, California: A re-evaluation of the Lake City fault zone: Geological Society of America Bulletin, v. 126, p. 523–531, doi:10.1130/B30785.1.

Fontiveros, V.C., 2010, 2D high-resolution seismic imaging of small-scale intrabasin faulting in Surprise Valley, California [M.S. thesis]: Stanford, California, Stanford University, 65 p.

Gaffney, E.S., Damjanac, B., and Valentine, G.A., 2007, Localization of volcanic activity: 2. Effects of pre-existing structure: Earth and Planetary Science Letters, v. 263, p. 323–338, doi:10.1016/j.epsl.2007.09.002.

Glen, J.M.G., Egger, A.E., Ippolito, C., and Athens, N., 2013, Correlation of geothermal springs with sub-surface fault terminations revealed by high-resolution, UAV-acquired magnetic data, *in* Proceedings of the 38th Workshop on Geothermal Reservoir Engineering: Stanford Geothermal Program Workshop Report SGP-TR-198, p. 1233–1242.

Grauch, V.J.S., and Hudson, M.R., 2007, Guides to understanding the aeromagnetic expression of faults in sedimentary

basins: Lessons learned from the central Rio Grande rift, New Mexico: Geosphere, v. 3, p. 596–623, doi:10.1130/GES00128.1.

Gudmundsson, A., 2002, Emplacement and arrest of sheets and dykes in central volcanoes: Journal of Volcanology and Geothermal Research, v. 116, p. 279–298, doi:10.1016/S0377-0273(02)00226-3.

Gudmundsson, A., 2003, Surface stresses associated with arrested dykes in rift zones: Bulletin of Volcanology, v. 65, p. 606–619, doi:10.1007/s00445-003-0289-7.

Hart, W.K., Aronson, J.L., and Mertzman, S.A., 1984, Areal distribution and age of low-K, high-alumina olivine tholeiite magmatism in the northwestern Great Basin: Geological Society of America Bulletin, v. 95, p. 186–195, doi:10.1130/0016-7606(1984)95<186:ADAAOL>2.0.CO;2.

Hedel, C.W., 1980, Late Quaternary faulting in western Surprise Valley, Modoc County, California [M.S. thesis]: San Jose, California, San Jose State University, 142 p.

Jablonski, H.W., 1974, World relative gravity reference network North America: U.S. Defense Mapping Agency Aerospace Center Reference Publication 25, 1261 p.

Keating, G.N., Valentine, G.A., Krier, D.J., and Perry, F.V., 2008, Shallow plumbing systems for small-volume basaltic volcanoes: Bulletin of Volcanology, v. 70, p. 563–582, doi:10.1007/s00445-007-0154-1.

Langenheim, V.E., Grow, J.A., Jachens, R.C., Dixon, G.L., and Miller, J.J., 2001, Geophysical constraints on the location and geometry of the Las Vegas Valley Shear Zone, Nevada: Tectonics, v. 20, p. 189–209, doi:10.1029/1999TC001159.

Lerch, D.W., Klemperer, S.L., Egger, A.E., Colgan, J.P., and Miller, E.L., 2010, The northwestern margin of the Basin-and-Range Province, part 1: Reflection profiling of the moderate-angle (~30°) Surprise Valley fault: Tectonophysics, v. 488, p. 143–149, doi:10.1016/j.tecto.2009.05.028.

Marrett, R., and Allmendinger, R.W., 1992, Amount of extension on "small" faults: An example from Viking graben: Geology, v. 20, p. 47–50, doi:10.1130/0091-7613(1992)020<0047:AOEOSF>2.3.CO;2.

Meigs, A., et al., 2009, Geological and geophysical perspectives on the magmatic and tectonic development, High Lava Plains and northwest Basin and Range, *in* O'Connor, J.E., et al., eds., Volcanoes to vineyards: Geologic field trips through the dynamic landscape of the Pacific Northwest: Geological Society of America Field Guide 15, p. 435–470, doi:10.1130/2009.fld015(21).

Okaya, D.A., and Thompson, G.A., 1985, Geometry of Cenozoic extensional faulting: Dixie Valley, Nevada: Tectonics, v. 4, p. 107–125, doi:10.1029/TC004i001p00107.

Pallister, J.S., et al., 2010, Broad accommodation of rift-related extension recorded by dyke intrusion in Saudi Arabia: Nature Geoscience, v. 3, p. 705–712, doi:10.1038/ngeo966.

Parsons, T., and Thompson, G.A., 1991, The role of magma overpressure in suppressing earthquakes and topography: Worldwide examples: Science, v. 253, p. 1399–1402, doi:10.1126/science.253.5026.1399.

Parsons, T., Thompson, G.A., and Smith, R.P., 1998, More than one way to stretch: A tectonic model for extension along the plume track of the Yellowstone hotspot and adjacent Basin and Range Province: Tectonics, v. 17, p. 221–234, doi:10.1029/98TC00463.

Payne, S.J., McCaffrey, R., and King, R.W., 2008, Strain rates and contemporary deformation in the Snake River Plain and surrounding Basin and Range from GPS and seismicity: Geology, v. 36, p. 647–650, doi:10.1130/G25039A.1.

Ponce, D.A., Glen, J.M.G., Egger, A.E., Bouligand, C., Watt, J.T., and Morin, R.L., 2009, Geophysical studies in the vicinity of Warner Mountains and Surprise Valley, northeast California, northwest Nevada, and southern Oregon: U.S. Geological Survey Open-File Report 2009-1157, 19 p.

Ritzinger, B.T., 2014, Paleomagnetic mapping of late Miocene–Pliocene basalt flows in the northwestern Basin and Range: Determining structural and topographic controls on the distribution of volcanic activity [M.S. thesis]: Ellensburg, Washington, Central Washington University, 45 p.

Scarberry, K.C., Meigs, A.J., and Grunder, A.L., 2010, Faulting in a propagating continental rift: Insight from the late Miocene structural development of the Abert Rim fault, southern Oregon, USA: Tectonophysics, v. 488, p. 71–86, doi:10.1016/j.tecto.2009.09.025.

Schultz, R.A., Mège, D., and Diot, H., 2008, Emplacement conditions of igneous dikes in Ethiopian Traps: Journal of Volcanology and Geothermal Research, v. 178, p. 683–692, doi:10.1016/j.jvolgeores.2008.08.012.

Strickley, D.J., 2014, Controls on fault geometry during early stages of extension in the Larkspur Hills, northwest Basin and Range [M.S. thesis]: Ellensburg, Washington, Central Washington University, 68 p.

U.S. Geological Survey and California Geological Survey, 2006, Quaternary Fault and Fold Database for the United States: http://earthquake.usgs.gov/hazards/qfaults/ (accessed January 2015).

Valentine, G.A., and Krogh, K.E.C., 2006, Emplacement of shallow dikes and sills beneath a small basaltic volcanic center—The role of pre-existing structure (Paiute Ridge, southern Nevada, USA): Earth and Planetary Science Letters, v. 246, p. 217–230, doi:10.1016/j.epsl.2006.04.031.

Warner, M., 1987, Migration—Why doesn't it work for deep continental data?: Royal Astronomical Society Geophysical Journal, v. 89, p. 21–26, doi:10.1111/j.1365-246X.1987.tb04382.x.

Wright, T.J., Ebinger, C., Biggs, J., Ayele, A., Yirgu, G., Keir, D., and Stork, A., 2006, Magma-maintained rift segmentation at continental rupture in the 2005 Afar dyking episode: Nature, v. 442, p. 291–294, doi:10.1038/nature04978.